BJC

Downregulation of EGFR in hypoxic, diffusion-limited areas of squamous cell carcinomas of the head and neck

Arnulf Mayer*,[1], Sebastian Zahnreich[1], Jürgen Brieger[2], Peter Vaupel[1] and Heinz Schmidberger[1]

[1]Department of Radiation Oncology and Radiotherapy, University Medical Center, Mainz 55131, Germany and [2]Department of Otolaryngology, Head and Neck Surgery, University Medical Center, Mainz 55131, Germany

Background: The receptor for the epidermal growth factor (EGFR) is widely considered to be one of the central drivers of oncogenesis in squamous cell carcinomas of the head and neck region (HNSCC). Inhibition of EGFR using monoclonal antibodies is established both in the curative and the palliative setting in this disease. HNSCCs are known to contain abundant hypoxic tissue areas and hypoxia has been shown to be involved in the (down)regulation of EGFR membrane expression.

Methods: A novel method for multiplex immunofluorescence and single-cell segmentation (via DAPI-stained nuclei) was established, to study the expression of EGFR, the endogenous hypoxia marker CA IX, and intratumoural diffusion distances from microvessels (using CD34 staining) in 58 human HNSCCs and 9 normal/cancer adjacent tissues.

Results: EGFR was found to be significantly downregulated with increasing distance from tumour microvessels, whereas the opposite was true for CA IX. Larger diffusion-limited areas were correlated with higher expression of CA IX.

Conclusions: The hypoxic tumour microenvironment may have a major role in mediating resistance against anti-EGFR strategies by downregulating EGFR molecules on tumour cells.

INTRODUCTION

Hypoxia is a major cause of treatment resistance of many solid malignant tumours (Wilson and Hay, 2011), particularly squamous cell carcinomas of the head and neck region (HNSCCs). A meta-analysis of almost 600 patients showed that the grand median oxygen partial pressure of these tumours is only 10 mm Hg, with more than one-fifth of the oxygen readings below 2.5 mm Hg (Vaupel and Mayer, 2007; Vaupel *et al*, 2007). Prospective, randomised studies have shown that hypoxic HNSCCs exhibit radioresistance, and curative chances of patients affected by these tumours benefit from therapeutic strategies that systematically address the problem of hypoxia-induced resistance to therapy, for example, by the use of hypoxic cell radiosenzitizers (Overgaard and Horsman, 1996).

A novel form of hypoxia-mediated treatment resistance may arise from the downregulation of molecules against which targeted anti-cancer therapies are aimed. Inhibition of the receptor for the epidermal growth factor (EGFR) using monoclonal antibodies is regarded as a prototype of targeted therapy. Indeed, tumours of the head and neck region are among the few entities in which an anti-EGFR strategy using the monoclonal antibody cetuximab has experienced widespread use in clinical practice since the landmark study by Bonner *et al* (2006, 2010). Recently published *in vitro* data have shown that the natural degradation cycle of EGFR is dependent upon a hypoxia-inducible protein, prolyl hydroxylase domain (PHD)-3. Under hypoxic conditions, EGFR signalling (i.e., phosphorylation of EGFR and ERK) was found to be significantly attenuated, a response that could be reversed by shRNA against PHD3 (Garvalov *et al*, 2014). A hypoxia-mediated downregulation of the EGFR-system seems biologically plausible as proliferative activity is handicapped under hypoxic conditions (Tannock, 1968). Consistently, EGFR expression is attenuated or missing in the distant cell layers of normal oral mucosa, as demonstrated by the

*Correspondence: Dr A Mayer; E-mail: arnmayer@uni-mainz.de

human protein atlas (www.proteinatlas.org) using five different anti-EGFR antibody clones (Uhlen *et al*, 2015). In HNSCC, different consequences of such downregulation of EGFR are conceivable. As active EGFR mediates radioresistance (Toulany and Rodemann, 2015), it could be hypothesised that hypoxia-mediated EGFR downregulation could lead to radiosensitization. However, this effect may be relativised by the fact that hypoxia *per se* is a well-known and strong radioprotective factor. Hence, the net effect could be a dormant state of the hypoxic cells with reduced or absent cell proliferation, which may render cancer cells less sensitive not only to radio- but also to chemotherapy. Cells with a reduced number of EGFR molecules on their cell surface would also be expected to be less sensitive to the direct cell death-promoting effects of cetuximab and may contribute less to any cetuximab-mediated immune stimulation. Hypoxia-mediated downregulation of EGFR thus appears to be of great clinical interest. In the present study, we have investigated a possible downregulation of EGFR expression by hypoxia in a diverse set of human HNSCC tissue specimens. A target protein of the hypoxia-inducible factor (HIF)-1, carbonic anhydrase (CA) IX, was used as a surrogate endogenous marker for tumour hypoxia. Using a novel protocol for multiparametric immunofluorescence in paraffin tissue sections, CA IX was stained together with EGFR, a marker for the microvascular endothelium (CD34) and DAPI in a multiplex design. Marker expression and spatial distribution were analysed using computerised morphometry based on single-cell segmentation.

PATIENTS AND METHODS

Patients and tissue specimens. Archived histological sections from 28 patients with HNSCC were obtained from the Department of Otolaryngology, Head and Neck Surgery, University Medical Center, Mainz. The study has been approved by the local medical ethics committee [Ethikkommission der Landesärztekammer Rheinland-Pfalz, No. 837.466.04(4624), 12.12.2008]. Furthermore, a set of HNSCC from 30 additional patients as well as normal and cancer adjacent tissues from 5 patients each were available in the form of duplicate 1.5 mm tissue cores on a commercial tissue microarray (HN801a, US Biomax, Rockville, MD, USA). Clinical data of all patients in the study, including the tissue microarray, are listed in Table 1.

Immunohistochemistry. Sections of 4–5 μm thickness were prepared from paraffin blocks using a high-precision microtome and dried overnight at 37 °C (Histology core facility, University Medical Center Mainz). On the next day, specimens were baked at 60 °C for 1 h, dewaxed in three changes of fresh xylene and then rehydrated in a descending alcohol series. Multichannel immunofluorescence detection was carried out using an adaptation of the method of Toth and Mezey (2007). In brief, initial retrieval of antigenic binding sites was performed by heating specimens in 10/1 mM Tris/EDTA pH 9.0 buffer in a microwave oven (Bosch HMT75M451, Robert Bosch GmbH, Munich, Germany) for 15 min. Primary antibodies were then incubated according to the conditions listed in Supplementary Table 1. Biotin-free, micro-polymer-based SuperPicture reagents (Thermo Fisher Scientific, Waltham, MA, USA) specifically directed against the species of origin of the primary antibodies were used for labelling the latter with horseradish peroxidase. Antigen visualisation was achieved by incubation with a panel of three different fluorochrome-tyramide conjugates in appropriate buffers following their activation with H_2O_2 (TSA detection kits, Thermo Fisher Scientific, see Supplementary Table 1 for fluorochromes used). Repeated microwave treatment between successive rounds of fluorescent staining was employed to completely quench peroxidase activity

Table 1. Clinical data for 58 patients in the study

	n
T stage	
1	5
2	22
3	12
4	12
x	7
N stage	
0	30
1	10
2a	1
2b	2
2c	6
x	9
M stage	
0	31
1	1
x	26
AJCC clinical stage	
I	3
II	12
III	13
IV	1
IVA	19
IVC	1
x	9
Grade	
0	2
1	14
2	23
3	15
x	4
Patient age	57 (34–81)

from the previous antigen-labelling step. As a final step, slides were incubated with DAPI at a concentration of 300 nM, covered with a coverslip using DAKO Fluorescence mounting medium (Dako Deutschland GmbH, Hamburg, Germany). Slides were dried overnight at 4 °C. Digital images of the specimens were acquired using fluorescence-equipped slidescanners (Pannoramic Confocal, 3D Histech, Budapest, Hungary and Axio Scan.Z1, Zeiss, Göttingen, Germany, both equipped with appropriate filter sets) at a resolution of 325 nm per pixel ($\sim 20 \times$ magnification in conventional microscopy). Only immunostaining compatible with the known biological function and corresponding subcellular localisation of each antigen was considered as being evaluable as marker expression (Supplementary Table 1).

Image analysis and data visualisation. Image analysis was carried out in entire microarray cores and in representative quadratic selections of equal horizontal diameter from the whole-slide specimens (1.5×1.5 mm). Small areas of the surrounding glass slide, overt necrosis and debris were excluded by manually defining masks for each image using Fiji/ImageJ (Schindelin *et al*, 2012). Segmentation of individual tumour cells was carried out in CellProfiler (Lamprecht *et al*, 2007) using a custom-designed algorithm ('analysis pipeline') which took the previously generated masks into account. The same algorithm also generated a CD34 threshold image representing the distribution of tumour blood vessels, which was cleaned using standard binary image filtering operations and then converted to a Euclidean Distance Map (EDM), in which each grey level value corresponds to the distance (in pixels) to the nearest microvessel. Subsequently, these grey level values were mathematically converted to a calibrated distance (in μm). Expression intensities of CA IX and EGFR were recorded

for each individual cell along with the positional information in the form of the mean grey level value of the EDM within the cell and all parameters were subsequently exported to FCS Express Plus 5 (*De Novo* Software, Glendale, CA, USA). FCS express was used to extract a set of custom parameters from the raw data which describe antigen-expression intensities (i.e., percentage of antigen-positive cells relative to all cells in a given section), the percentage of cells beyond $80\,\mu m$ and $120\,\mu m$, respectively, from the nearest microvessel relative to all cells (i.e., the diffusion-limited fractions (DLF) beyond $80\,\mu m$ and $120\,\mu m$, respectively, DLF_{80} and DLF_{120}) and the relationship between antigen-expression intensities and the distance from the nearest tumour microvessel (see Supplementary Table 2). For the latter analysis, we defined three classes of diffusion distances around microvessels: $0-80\,\mu m$ ('near'), $81-120\,\mu m$ ('intermediate'), and $>120\,\mu m$ ('distant') and calculated differences between the expression of EGFR and CA IX in near, intermediate and distant classes using Wilcoxon's test for paired samples. These differences were only calculated when at least 1% of all tumour cells were positive for the respective antigens to minimise the impact of minor staining artefacts on quantitative results. The details of the analysis procedure are shown in Supplementary Figure 1.

Statistical analysis. All statistical tests were performed using the SPSS software package (Version 23, IBM, Armonk, NY, USA). The significance level was set at $\alpha = 5\%$ for all comparisons. Linear correlations between two variables were described by Spearman's rank correlation coefficient (ρ). A two-sided Wilcoxon's test for paired samples was used for the analysis of the mean differences between EGFR and CA IX in the three diffusion classes.

Illustrations. Figures 1, 4 and 5 and Supplementary Figures 1–3 contain subregions taken from the original slidescanner files and were brightness-, grey level- and gamma-adjusted to maximise visibility of antigen-expression patterns. These modifications were applied solely for the purpose of illustration, whereas only unmodified 8- bit TIFF images were used for quantitative analyses. Image annotations were made using Image Pro Premier (Version 9.1.4, Media Cybernetics, Rockville, MD, USA) and Adobe Photoshop CC 2015 (Adobe, San José, CA, USA). Multi-panel figures were constructed using the ScientiFig (Aigouy and Mirouse, 2013) and FigureJ (Mutterer and Zinck, 2013) plugins for ImageJ as well as Adobe Illustrator CC 2015 (Adobe). The boxplot shown in Figure 3 was created using SigmaPlot 11.

RESULTS

Specimens eligible for analysis. Diffusion distances, CA IX and EGFR expression were evaluable in 118 subregions/microarray cores ($1.5 \times 1.5\,mm$) from 58 HNSCCs (28 whole slide- and 30 tissue microarray-specimens, corresponding to 2 subregions for each patient in the vast majority of cases, and 1 or 3 subregions in a small minority). The aforementioned parameters were also evaluable in cancer adjacent tissue in 4 of 5 patients (i.e., in 6 of 10 microarray cores) and normal head and neck tissue in 5 patients (i.e., in 7 of 10 cores). Reasons for the exclusion of some specimens from the analysis were loss of tumour tissue from the glass slide or obscuration of fluorescent signals by substantial artefacts.

Overall expression intensity of EGFR and CA IX. The intensity of EGFR expression was weak in 38.1% (0–5% of cells positive), moderate in 30.5% (>5–20% of cells positive) and strong in 31.4% of all human tumours ($>20\%$ positive cells). The respective numbers for CA IX were 71.2%, 17.8% and 11.0%. Expression of EGFR was observed in all but one normal and cancer adjacent tissue specimens (0–41.2% of cells positive, see Supplementary Figure 2 for an example). Conversely, CA IX expression was almost completely absent in normal/cancer adjacent tissue. Only one (of 13) specimens showed 6% CA IX-positive cells.

Downregulation of EGFR with increasing distance from microvessels. In most tumour specimens investigated in this study it was visually evident that the expression of EGFR was decreasing with increasing distance of the cells from the nearest microvessels (Figure 1). A substantial decrease in EGFR expression intensity was typically observed beyond a distance of $80\,\mu m$ relative to the nearest microvessel. To objectify this subjective impression, we analysed the expression of EGFR and CA IX in the three classes of diffusion distances around microvessels ($0-80\,\mu m$ ('near'), $81-120\,\mu m$ ('intermediate') and $>120\,\mu m$ ('distant')). A typical example of this analysis is shown in Supplementary Figure 1. According to the criterion of at least 1% antigen-positive cells, 83 subregions/cores from 44 patients could be analysed for EGFR and 59 subregions/cores from 37 patients for CA IX. A pooled analysis (see Figure 2) showed statistically significant downregulation of EGFR in near *vs* intermediate, near *vs* distant and intermediate *vs* distant categories ($P<0.00001$ for all three). Conversely, CA IX was found to be upregulated in distant *vs* near ($P=0.001$) and distant *vs* intermediate ($P<0.00001$) categories, but not, in intermediate *vs* near ($P=0.538$) categories. Overall, these data strongly support our hypothesis of a downregulation of EGFR and an upregulation of CA IX with increasing distance from microvessels.

Correlations between DLF and CA IX expression. The fractions of tissue beyond a diffusion distance of 80 and $120\,\mu m$ (DLF_{80} and DLF_{120}, respectively) showed significant positive correlation with the percentage of cells positive for CA IX (Peason's $r=0.421$, $P=0.00002$, and $r=0.372$, $P=0.00003$, respectively, Figure 3). The fact that the strength of these correlations was moderate at best was partially due to the fact that many of the specimens investigated contained unequivocally diffusion-limited areas which did not show CA IX expression despite the presence of CA IX signal in other areas of the same specimens (i.e., a positive internal control), corresponding to a 'hypoxia-anergic' behaviour of CA IX in such tissue subvolumes (Figure 4 shows a pointed example). Conversely, non-diffusion-limited tissue areas with strong CA IX staining existed but were rarer. Interestingly, in one instance, CA IX signal in tumour cells directly adjacent to blood vessels could be traced back to the fact that these vessel segments were situated at the turn of elongated 'hairpin'-like microvessels (Figure 5), a structural abnormality of blood vessels in solid tumours which is known, for example, from corrosion cast studies (Konerding *et al*, 2001). Owing to the phenomenon of countercurrent exchange of oxygen in afferent and efferent limbs of the supplying capillaries, such distant ends cannot adequately supply oxygen even to cells situated directly adjacent to them.

Correlations with clinical and histopathologic data. These analyses were carried out in an aggregated data set in which all calculations were carried out per patient ($n=58$). DLF_{80} and DLF_{120} were both inversely correlated with n-stage ($r=-0.42$, $P=0.002$ and $r=-0.39$, $P=0.006$, respectively). Tumour grading showed a weak direct correlation with CA IX expression ($r=0.3$, $P=0.027$). A weak correlation was also found between the established prognostic factors tumour grade and n-stage ($r=0.31$, $P=0.033$).

DISCUSSION

The central finding of the present study is a systematically weaker expression of EGFR in diffusion-limited areas of human HNSCC. To demonstrate this, we have established a novel method of multiplex immunofluorescence in conjunction with single-cell-based image
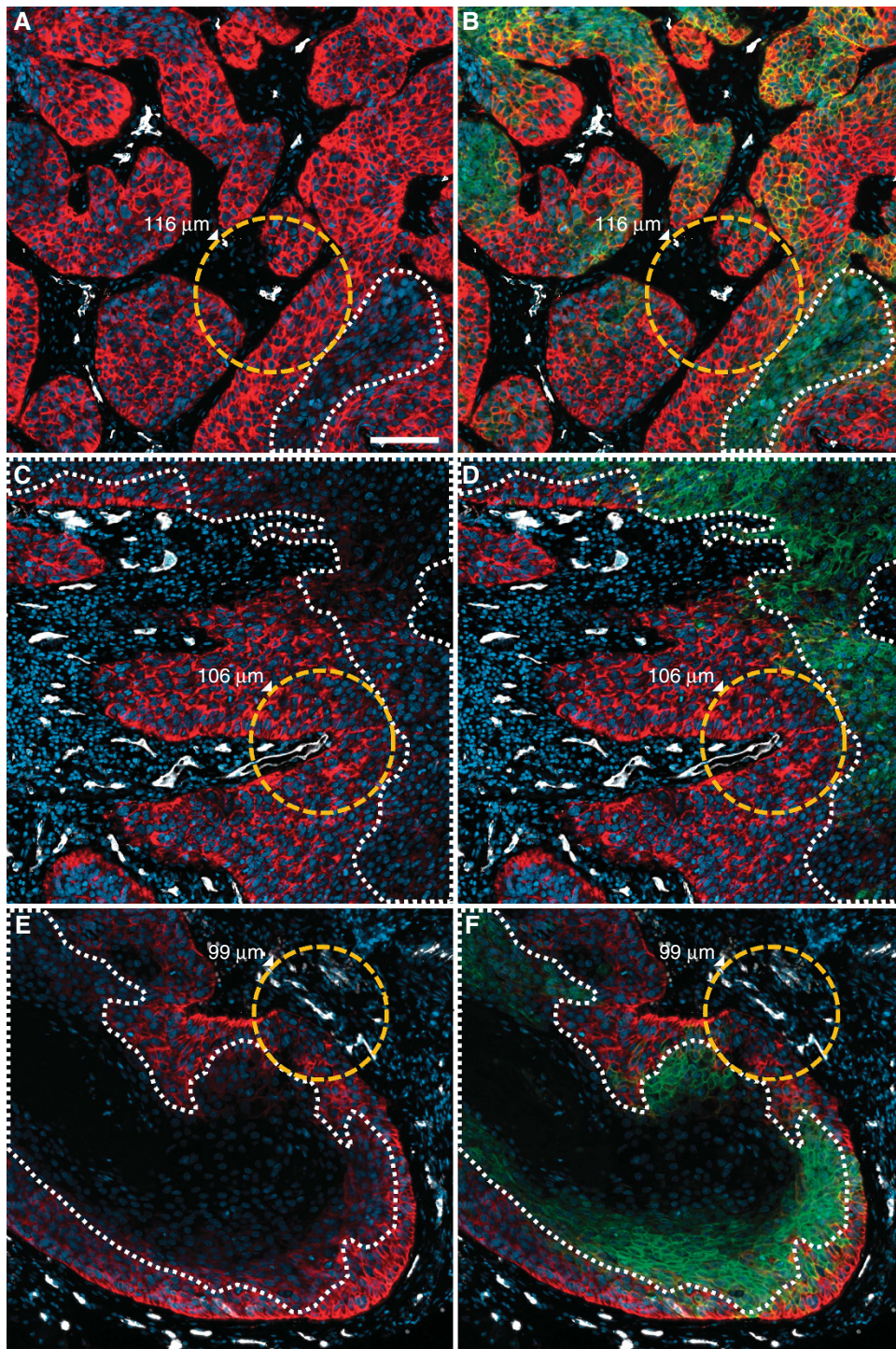
Figure 1. Decreasing expression of EGFR with increasing distance from the nearest microvessel. Examples from three different patients (upper, middle and lower rows) illustrate that EGFR-negative tumour areas (dotted white lines in **A**, **C**, **E**) are situated at the distances indicated relative to the nearest tumour blood vessel (dotted orange lines and corresponding values of the diffusion radii). **B**, **D** and **F** show widespread expression of CA IX in the aforementioned diffusion-limited areas.

analysis. One of the central strengths of this technical approach is the possibility to freely choose arbitrary combinations of mono-clonal primary antibodies against protein targets of interest. Regarding EGFR, a broad palette of monoclonal primary antibodies suitable for immunohistochemistry on paraffin sections is available and has been used in conjunction with a variety of immunohistochemical staining protocols in a large number of clinical biomarker studies. However, these investigations yielded substantially heterogeneous results with regard to the percentage of EGFR-positive and -negative tumours as well as the clinical impact of EGFR expression (see Supplementary Table 3, which extends upon the meta-analysis of Zhu *et al* (2013)). Accordingly, there is currently no single monoclonal antibody against EGFR which is considered to be a gold standard. Conversely, to the best of our knowledge, there is also only one monoclonal anti-EGFR antibody, for which extensive quantitative validation showed direct

correlations between expression levels in quantitative immuno-fluorescence (Aqua method) and protein abundance in cell-/tissue-extracts using quantitative western blotting, which is the rabbit monoclonal antibody clone D38B1 (Dimou *et al*, 2011). Consequently, this antibody was chosen for the present study and yielded strong and biologically plausible staining with our multiplex method (see Figures 1 and 2). EGFR detection using this method also showed an impressive dynamic range which was particularly evident in a single human tumour, in which a spatially confined, cohesive subpopulation of tumour cells showed very strong expression of EGFR, whereas the rest of the neoplastic epithelial cells only exhibited a weak, but nevertheless still clearly membranous antigen-expression pattern (Supplementary Figure. 3). Stronger expression of EGFR closer to microvessels in cancers of the head and neck region has been described before by Stegeman *et al* (2012, 2013), although these authors did not analyse the phenomenon in a quantitative fashion. However, other data from the Nijmegen group pointed towards an expression of EGFR within the tumours that was 'more diffuse' and 'with the highest expression levels at intermediate distances from the blood vessels' (Hoogsteen *et al*, 2012). Furthermore, a collaborative study from Dresden and Nijmegen (Santiago *et al*, 2010) using FaDu xenograft tumours even showed a homogenous distribution of EGFR which lacked differences between hypoxic and non-hypoxic tumour areas. An older study from Dresden (Petersen *et al*, 2003) examined the time course of EGFR expression during fractionated radiotherapy and even though these authors did not specifically examine a possible differential expression of EGFR in (Pimonidazole-positive) hypoxic areas, they found a pronounced downregulation of EGFR membrane expression between days 12 and 18 of the irradiation series, concurrent with the lowest extent of hypoxic areas in the tumours and, thus, incongruous to what would have been expected on the basis of the data of our study. Conversely, an older study in breast cancer had shown an inverse correlation between EGFR and VEGF expression (Leek *et al*, 2000). These latter data again point in the same direction as our results, as VEGF is a HIF-1 target gene and can be induced by hypoxia. Interestingly, all of the aforementioned studies agree that there at least seems to be no upregulation of EGFR in hypoxic tumour areas, thereby

contradicting the findings of Franovic *et al* (2007), who showed a strong upregulation of EGFR in a number of different cell types under hypoxic conditions. This effect was shown to be mediated by HIF-2α, a finding which was later corroborated by additional data from the same group (Franovic *et al*, 2009). However, no head and neck cancer cell lines were tested in these studies and in yet another later study, hypoxia-mediated upregulation of EGFR was indeed not found to occur in a number of head and neck cancer cell lines, even though hypoxia-induced activation of EGFR downstream signalling did occur in two of these cell lines (Wang and Schneider, 2010). Although different methodologies, for example, different anti-EGFR antibodies (monoclonal *vs* polyclonal) and staining techniques may explain some of the different
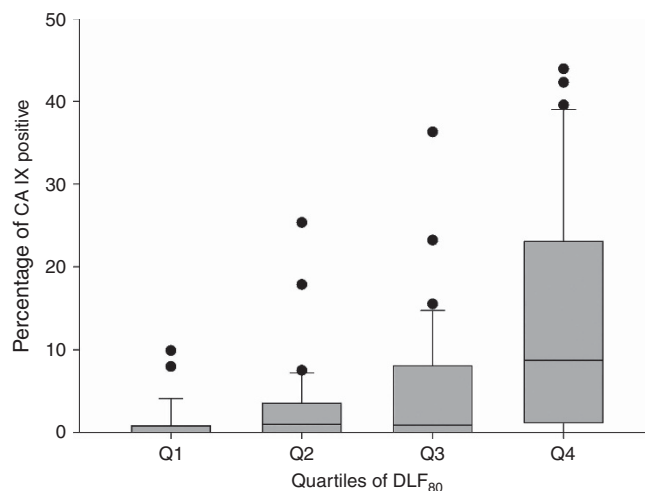

Figure 3. Correlation between DLF_{80} and CA IX expression. The percentage of cells positive for CA IX increases in ascending quartiles of the percentage of cells beyond a distance of 80 μm from the nearest microvessel in a given specimen, that is, the DLF > 80 μm, DLF_{80} (Q1–Q4).
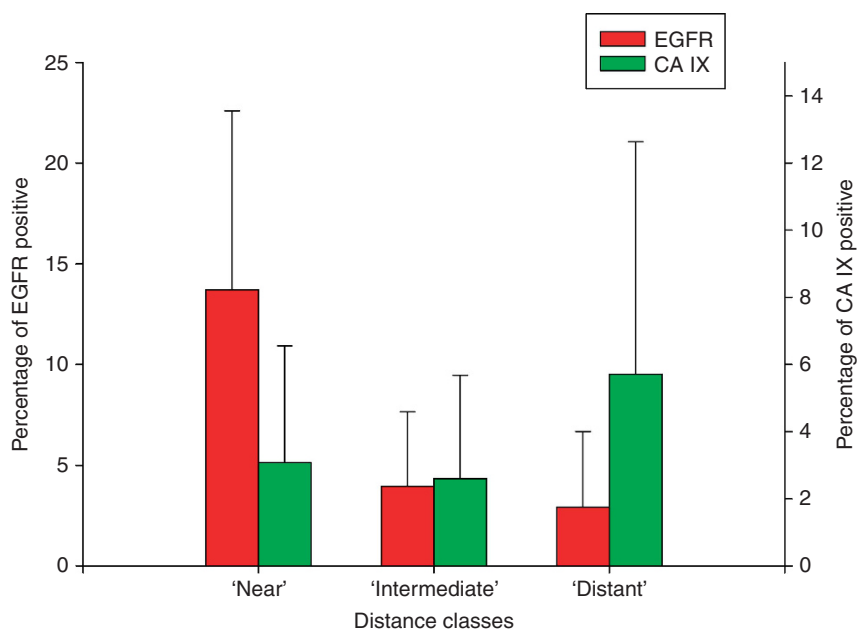

Figure 2. Pooled analysis of the differential expression of EGFR and CA IX in three distance classes relative to the nearest tumour microvessel. EGFR was higher in near *vs* intermediate, near *vs* distant and intermediate *vs* distant classes (P < 0.00001 for all three), whereas CA IX was higher in distant *vs* near and distant *vs* intermediate classes (P = 0.01 and P < 0.00001, respectively). Error bars indicate the s.d.

results found in the IHC studies, the provocatory findings in some cell culture studies of EGFR upregulation under hypoxia cannot be explained on the basis of the data of our study.

Our finding of 31.4% of strongly EGFR-positive tumours is higher than recently reported for amplification/mutation and protein overexpression in the cancer genome atlas (TCGA) cohort (15%), but lower than what many other published studies have found (see Supplementary Table 3). Interestingly, the TCGA analysis had also revealed that EGFR is probably a driver mutation only in a minority of tumours, whereas oncogenesis in HNSCC seems to be dependent upon mutations of the PI3 kinase (PI3K) in a larger percentage of cases, making it less and less advisable to continue treating patients with anti-EGFR antibodies without prior testing of their individual mutation status (Cancer Genome Atlas Network, 2015).

Downregulation of EGFR in hypoxic tumour areas is not only mechanistically explainable by the upregulation of hypoxia-inducible PHD-3 as outlined above, but also biologically plausible because (EGFR-induced) cell proliferation is expected to depend upon sufficient oxygen supply. Nevertheless the evidence presented here is so far only correlative and it may well be that the weaker expression of EGFR observed in diffusion-limited areas of the specimens is not caused by hypoxia itself or by hypoxia alone but may instead be the consequence of a lack of other nutrients (e.g., glucose), local accumulation of metabolic waste products
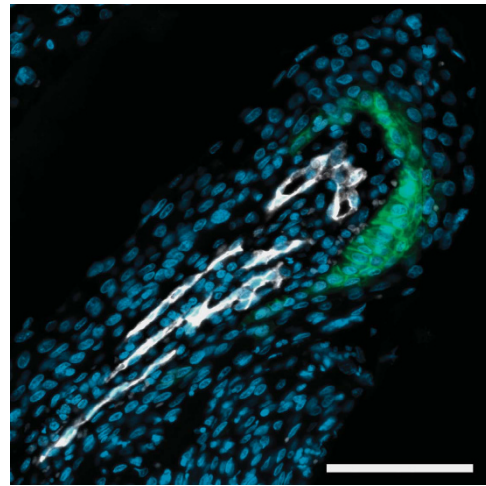

Figure 5. Perivascular CA IX expression at the distal end of elongated capillaries. Depicted are elongated capillaries running from the lower left corner of the image towards the upper right corner and making a hairpin-like turn at the tip. Consistent with the concept of a countercurrent oxygen exchange (oxygen diffusion shunt) between arterial and venous limbs of these capillaries, CA IX-positive cells are observed at the tip of the hairpin.
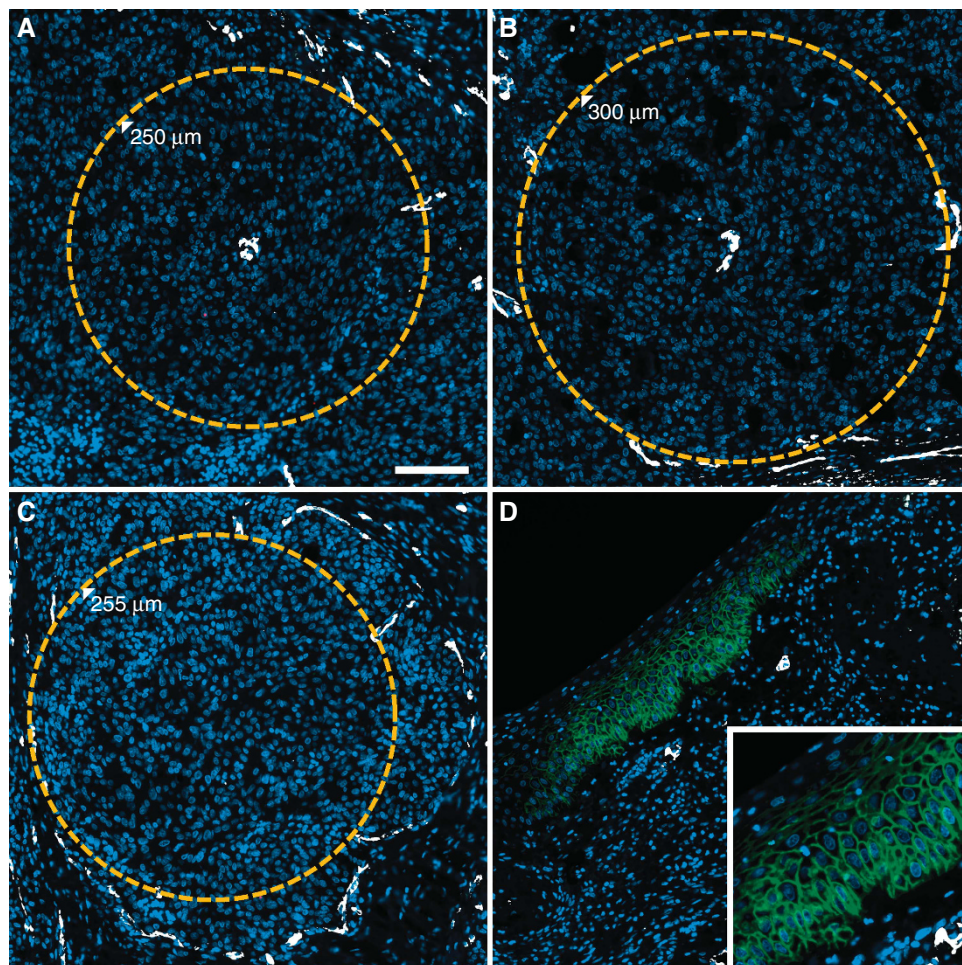

Figure 4. 'Hypoxia-anergic' phenotype without CA IX expression despite enlarged diffusion distances. (A and **B)** Subregions of one tumour specimen exhibiting enlarged diffusion distances around individual microvessels (orange circles, numbers denote radii). **(C)** a large avascular region from the same tumour surrounded by sparse microvessels (orange circle, number denotes radius). **(A–C)** show paradoxical absence of CA IX expression in diffusion-limited regions despite the presence of a positive internal control for CA IX detection in cancer adjacent epithelium present within the same specimen **(D)**, inset shows membranous expression pattern of CA IX). Scale bar in **A**, 100 μm.

(e.g., lactate), extracellular acidosis or even complex combinations of the aforementioned factors. In fact, a recent *in vitro* study in three cetuximab-sensitive HNSCC cell lines indicated that hypoxia alone did not interfere with the efficacy of this drug (Boeckx *et al*, 2015). We have also not systematically analysed EGFR activity in this study, because this would have required investigation of expression and phosphorylation patterns of a plethora of down-stream target molecules. Nevertheless, a preliminary analysis of the expression of phosphorylated ribosomal protein S6 (Ser235/236), a well-accepted down-stream target of the PI3K-AKT-mTOR pathway and the EGFR (Psyrri *et al*, 2013), did indeed show the expected pattern of a preferential expression adjacent to blood vessels (see Supplementary Figure 4).

A second finding of importance of our study is the existence of a correlation of the size of diffusion-limited areas (DLFs) and the expression of the hypoxia-associated endogenous marker CA IX. Increasing expression intensity of CA IX with increasing distance from microvessels was not only evident visually in many of the specimens investigated in this series, but could also be objectified in a quantative analysis (see Figure 2). This finding was not necessarily to be expected as we (Mayer *et al*, 2005) and others (Hedley *et al*, 2003; Iakovlev *et al*, 2007) have reported a lack of correlation between CA IX expression and invasive pO_2 measurements using the Eppendorf polarographic microelectrode system in cancers of the uterine cervix. Indeed, many examples of both missing CA IX expression in clearly diffusion-limited areas (i.e., expected to be hypoxic) and expression of CA IX in presumptively normoxic regions directly adjacent to microvessels were found in our study. Our multichannel fluorescence images show that the latter may in part be caused by the exhaustion of oxygen supply along the longitudinal axis of elongated tumour microvessels. This mechanism may lead to a situation in which the distant hairpin turn of such microvessels has oxygen partial pressures comparable to venous blood and, therefore, cannot adequately supply even those tumour cells which are directly adjacent to such parts of tumour blood vessels. We were able to directly visualise this pathophysiology (Figure 5), which has traditionally been inferred from anatomical studies (Konerding *et al*, 2001; Vaupel and Mayer, 2014). It is tempting to speculate that other blood vessels which were visually unaltered and thus not excluded from our algorithm which calculates diffusion distances may be in fact blind ends of capillaries or may be situated at the border of tumour micronecroses and thus be non-functional. Furthermore, expression of CA IX adjacent to blood vessels may also be the consequence of acute hypoxia, that is, temporal flow stop or perfusion with plasma only (Vaupel and Mayer, 2014). Conversely, a lack of CA IX expression in diffusion-limited areas of the specimen may be caused by insufficient activation of the HIF-system in some tumours as the authors have shown in a prior study that benign leiomyomas do not activate the HIF-system (and do not show expression of CA IX) despite the fact that these tumours are severely hypoxic, as measured with polarographic needle electrodes (Mayer *et al*, 2008). Finally, some of the discrepancies seen between the extent of diffusion-limited areas and CA IX may also have methodological reasons, for example, overall weaker staining in specimens which may have been fixed according to different protocols (e.g., higher formalin concentration, buffered *vs* unbuffered formalin, extended fixation times) without this fact being acknowledeged to us or false-positive 'perivascular' staining in cases where small artefacts may have been misinterpreted by our algorithm as blood vessels. Despite rigorous methodology, these factors cannot be excluded completely.

It has also been interesting to see that better vascularised tumours with smaller DLFs had a higher propensity for lymph node metastases, whereas higher grading was correlated directly with the expression of the hypoxia-associated marker CA IX. Correlations between higher vascularity of cancers of the head and

neck region and the lymph node metastases have been described by other authors, for example, by Kyzas *et al* (2006) using IHC staining for CD105/endoglin and by Delorme *et al* (1997) using colour Doppler sonography. Although correlations between tumour grading and CA IX expression have been reported for other tumour entities, for example, in our study in high-grade gliomas (Mayer *et al*, 2012), there seem to be no positive data in head and neck cancer. Although we do not have follow-up data for the tumours investigated in this study we plan to investigate the relevance of the markers assessed here in the future in a cohort of 111 patients treated with definitive chemoradiotherapy (with or without induction chemotherapy) at our institution since 2006.

In summary, we have established a novel method of multi-parametric immunofluorescence in combination with quantitative single-cell-based image analysis to demonstrate a downregulation of EGFR in diffusion-limited and often CA IX-positive areas of HNSCC. In patients treated with combinations of radiotherapy and anti-EGFR antibodies, downregulation of EGFR may mediate resistance against both modalities and may thus lead to tumour recurrence. Further research into the field of the modification of molecular targets by the tumour microenvironment is clearly warranted.

CONFLICT OF INTEREST

The authors declare no conflict of interest.

REFERENCES

Aigouy B, Mirouse V (2013) ScientiFig: a tool to build publication-ready scientific figures. *Nat Methods* **10**(11): 1048.

Boeckx C, Van den Bossche J, De Pauw I, Peeters M, Lardon F, Baay M, Wouters A (2015) The hypoxic tumor microenvironment and drug resistance against EGFR inhibitors: preclinical study in cetuximab-sensitive head and neck squamous cell carcinoma cell lines. *BMC Res Notes* **8**: 203.

Bonner JA, Harari PM, Giralt J, Azarnia N, Shin DM, Cohen RB, Jones CU, Sur R, Raben D, Jassem J, Ove R, Kies MS, Baselga J, Youssoufian H, Amellal N, Rowinsky EK, Ang KK (2006) Radiotherapy plus cetuximab for squamous-cell carcinoma of the head and neck. *N Engl J Med* **354**(6): 567–578.

Bonner JA, Harari PM, Giralt J, Cohen RB, Jones CU, Sur RK, Raben D, Baselga J, Spencer SA, Zhu J, Youssoufian H, Rowinsky EK, Ang KK (2010) Radiotherapy plus cetuximab for locoregionally advanced head and neck cancer: 5-year survival data from a phase 3 randomised trial, and relation between cetuximab-induced rash and survival. *Lancet Oncol* **11**(1): 21–28.

Cancer Genome Atlas Network (2015) Comprehensive genomic characterization of head and neck squamous cell carcinomas *Nature* **517**(7536): 576–582.

Delorme S, Dietz A, Rudat V, Zuna I, Bahner ML, van Kaick G (1997) Prognostic significance of color Doppler findings in head and neck tumors. *Ultrasound Med Biol* **23**(9): 1311–1317.

Dimou A, Agarwal S, Anagnostou V, Viray H, Christensen S, Gould Rothberg B, Zolota V, Syrigos K, Rimm DL (2011) Standardization of epidermal growth factor receptor (EGFR) measurement by quantitative immunofluorescence and impact on antibody-based mutation detection in non-small cell lung cancer. *Am J Pathol* **179**(2): 580–589.

Franovic A, Gunaratnam L, Smith K, Robert I, Patten D, Lee S (2007) Translational up-regulation of the EGFR by tumor hypoxia provides a

nonmutational explanation for its overexpression in human cancer. *Proc Natl Acad Sci USA* **104**(32): 13092–13097.

Franovic A, Holterman CE, Payette J, Lee S (2009) Human cancers converge at the HIF-2α oncogenic axis. *Proc Natl Acad Sci USA* **106**(50): 21306–21311.

Garvalov BK, Foss F, Henze AT, Bethani I, Graf-Hochst S, Singh D, Filatova A, Dopeso H, Seidel S, Damm M, Acker-Palmer A, Acker T (2014) PHD3 regulates EGFR internalization and signalling in tumours. *Nat Commun* **5**: 5577.

Hedley D, Pintilie M, Woo J, Morrison A, Birle D, Fyles A, Milosevic M, Hill R (2003) Carbonic anhydrase IX expression, hypoxia, and prognosis in patients with uterine cervical carcinomas. *Clin Cancer Res* **9**(15): 5666–5674.

Hoogsteen IJ, Marres HA, van den Hoogen FJ, Rijken PF, Lok J, Bussink J, Kaanders JH (2012) Expression of EGFR under tumor hypoxia: identification of a subpopulation of tumor cells responsible for aggressiveness and treatment resistance. *Int J Radiat Oncol Biol Phys* **84**(3): 807–814.

Iakovlev VV, Pintilie M, Morrison A, Fyles AW, Hill RP, Hedley DW (2007) Effect of distributional heterogeneity on the analysis of tumor hypoxia based on carbonic anhydrase IX. *Lab Invest* **87**(12): 1206–1217.

Konerding MA, Fait E, Gaumann A (2001) 3D microvascular architecture of pre-cancerous lesions and invasive carcinomas of the colon. *Br J Cancer* **84**(10): 1354–1362.

Kyzas PA, Agnantis NJ, Stefanou D (2006) Endoglin (CD105) as a prognostic factor in head and neck squamous cell carcinoma. *Virchows Arch* **448**(6): 768–775.

Lamprecht MR, Sabatini DM, Carpenter AE (2007) CellProfiler: free, versatile software for automated biological image analysis. *Biotechniques* **42**(1): 71–75.

Leek RD, Hunt NC, Landers RJ, Lewis CE, Royds JA, Harris AL (2000) Macrophage infiltration is associated with VEGF and EGFR expression in breast cancer. *J Pathol* **190**(4): 430–436.

Mayer A, Hockel M, Vaupel P (2005) Carbonic anhydrase IX expression and tumor oxygenation status do not correlate at the microregional level in locally advanced cancers of the uterine cervix. *Clin Cancer Res* **11**(20): 7220–7225.

Mayer A, Höckel M, Wree A, Leo C, Horn LC, Vaupel P (2008) Lack of hypoxic response in uterine leiomyomas despite severe tissue hypoxia. *Cancer Res* **68**(12): 4719–4726.

Mayer A, Schneider F, Vaupel P, Sommer C, Schmidberger H (2012) Differential expression of HIF-1 in glioblastoma multiforme and anaplastic astrocytoma. *Int J Oncol* **41**(4): 1260–1270.

Mutterer J, Zinck E (2013) Quick-and-clean article figures with FigureJ. *J Microsc* **252**(1): 89–91.

Overgaard J, Horsman MR (1996) Modification of hypoxia-induced radioresistance in tumors by the use of oxygen and sensitizers. *Semin Radiat Oncol* **6**(1): 10–21.

Petersen C, Eicheler W, Frommel A, Krause M, Balschukat S, Zips D, Baumann M (2003) Proliferation and micromilieu during fractionated irradiation of human FaDu squamous cell carcinoma in nude mice. *Int J Radiat Biol* **79**(7): 469–477.

Psyrri A, Seiwert TY, Jimeno A (2013) Molecular pathways in head and neck cancer: EGFR, PI3K, and more. *Am Soc Clin Oncol Educ Book* 246–255.

Santiago A, Eicheler W, Bussink J, Rijken P, Yaromina A, Beuthien-Baumann B, van der Kogel AJ, Baumann M, Krause M (2010) Effect of cetuximab and fractionated irradiation on tumour micro-environment. *Radiother Oncol* **97**(2): 322–329.

Schindelin J, Arganda-Carreras I, Frise E, Kaynig V, Longair M, Pietzsch T, Preibisch S, Rueden C, Saalfeld S, Schmid B, Tinevez JY, White DJ, Hartenstein V, Eliceiri K, Tomancak P, Cardona A (2012) Fiji: an open-source platform for biological-image analysis. *Nat Methods* **9**(7): 676–682.

Stegeman H, Kaanders JH, van der Kogel AJ, Iida M, Wheeler DL, Span PN, Bussink J (2013) Predictive value of hypoxia, proliferation and tyrosine kinase receptors for EGFR-inhibition and radiotherapy sensitivity in head and neck cancer models. *Radiother Oncol* **106**(3): 383–389.

Stegeman H, Kaanders JH, Wheeler DL, van der Kogel AJ, Verheijen MM, Waaijer SJ, Iida M, Grenman R, Span PN, Bussink J (2012) Activation of AKT by hypoxia: a potential target for hypoxic tumors of the head and neck. *BMC Cancer* **12**: 463.

Tannock IF (1968) The relation between cell proliferation and the vascular system in a transplanted mouse mammary tumour. *Br J Cancer* **22**(2): 258–273.

Toth ZE, Mezey E (2007) Simultaneous visualization of multiple antigens with tyramide signal amplification using antibodies from the same species. *J Histochem Cytochem* **55**(6): 545–554.

Toulany M, Rodemann HP (2015) Phosphatidylinositol 3-kinase/Akt signaling as a key mediator of tumor cell responsiveness to radiation. *Semin Cancer Biol* **35**: 180–190.

Uhlen M, Fagerberg L, Hallstrom BM, Lindskog C, Oksvold P, Mardinoglu A, Sivertsson A, Kampf C, Sjostedt E, Asplund A, Olsson I, Edlund K, Lundberg E, Navani S, Szigyarto CA, Odeberg J, Djureinovic D, Takanen JO, Hober S, Alm T, Edqvist PH, Berling H, Tegel H, Mulder J, Rockberg J, Nilsson P, Schwenk JM, Hamsten M, von Feilitzen K, Forsberg M, Persson L, Johansson F, Zwahlen M, von Heijne G, Nielsen J, Ponten F (2015) Proteomics. Tissue-based map of the human proteome. *Science* **347**(6220): 1260419.

Vaupel P, Höckel M, Mayer A (2007) Detection and characterization of tumor hypoxia using pO$_2$ histography. *Antioxid Redox Signal* **9**(8): 1221–1235.

Vaupel P, Mayer A (2007) Hypoxia in cancer: significance and impact on clinical outcome. *Cancer Metastasis Rev* **26**(2): 225–239.

Vaupel P, Mayer A (2014) Hypoxia in tumors: pathogenesis-related classification, characterization of hypoxia subtypes, and associated biological and clinical implications. *Adv Exp Med Biol* **812**: 19–24.

Wang X, Schneider A (2010) HIF-2alpha-mediated activation of the epidermal growth factor receptor potentiates head and neck cancer cell migration in response to hypoxia. *Carcinogenesis* **31**(7): 1202–1210.

Wilson WR, Hay MP (2011) Targeting hypoxia in cancer therapy. *Nat Rev Cancer* **11**(6): 393–410.

Zhu X, Zhang F, Zhang W, He J, Zhao Y, Chen X (2013) Prognostic role of epidermal growth factor receptor in head and neck cancer: a meta-analysis. *J Surg Oncol* **108**(6): 387–397.

Supplementary Information accompanies this paper on British Journal of Cancer website (http://www.nature.com/bjc)